

AD-A179 611

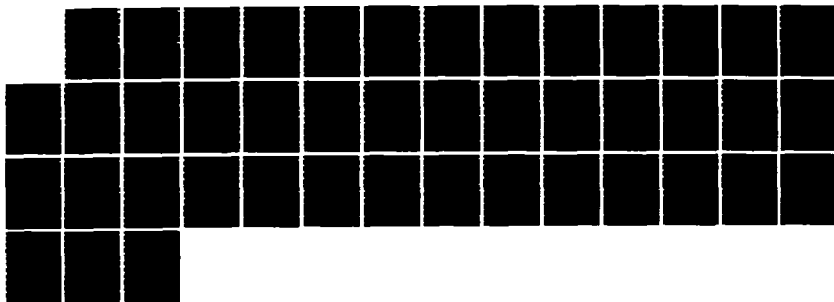
STUDY TO DEVELOP USE OF GRAVITY GRADIMETERS IN GRAVITY
MAPPING(U) STANFORD UNIV CALIF GUIDANCE AND CONTROL LAB
D DEBRA ET AL FEB 86 AFGL-TR-86-0166 F19628-82-K-0042

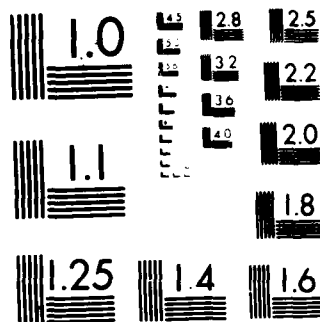
1/1

UNCLASSIFIED

F/G 8/5

NL





MICROCOPY RESOLUTION TEST CHART
NATIONAL BUREAU OF STANDARDS-1963-A

AFGL-TR-86-0166

1:2
REF ID: A61166

Study to Develop Use of Gravity Gradiometers
in Gravity Mapping

Daniel DeBra
John Breakwell

Stanford University
Guidance and Control Laboratory
Department of Aeronautics & Astronautics
Stanford, CA 94305

February 1986

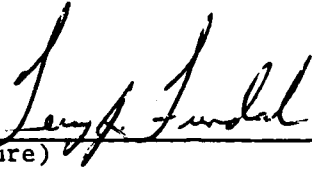
Final Report
28 April 1982 - 31 October 1985

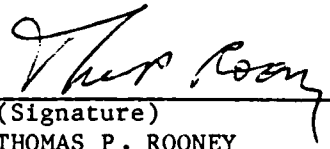
APPROVED FOR PUBLIC RELEASE; DISTRIBUTION UNLIMITED

AIR FORCE GEOPHYSICS LABORATORY
AIR FORCE SYSTEMS COMMAND
UNITED STATES AIR FORCE
HANSCOM AIR FORCE BASE, MASSACHUSETTS 01731

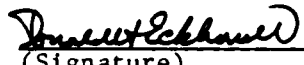
AD-A179 611

This technical report has been reviewed and is approved for publication.


(Signature)
TERRY J. FUNDAK
Contract Manager


(Signature)
THOMAS P. ROONEY
Branch Chief

FOR THE COMMANDER


(Signature)
DONALD H. ECKHARDT
Division Director

This report has been reviewed by the ESD Public Affairs Office (PA) and is releasable to the National Technical Information Services (NTIS).

Qualified requestors may obtain additional copies from the Defense Technical Information Center. All others should apply to the National Technical Information Service.

If your address has changed, or if you wish to be removed from the mailing list, or if the addressee is no longer employed by your organization, please notify AFGL/DAA, Hanscom AFB, MA 01731. This will assist us in maintaining a current mailing list.

Do not return copies of this report unless contractual obligations or notices on a specific document requires that it be returned.

Unclassified

SECURITY CLASSIFICATION OF THIS PAGE (When Data Entered)

REPORT DOCUMENTATION PAGE		READ INSTRUCTIONS BEFORE COMPLETING FORM
1. REPORT NUMBER AFGL-TR-86-0166	2. GOVT ACCESSION NO.	3. RECIPIENT'S CATALOG NUMBER
4. TITLE (and Subtitle) Study to Develop use of Gravity Gradiometers in Gravity Mapping		5. TYPE OF REPORT & PERIOD COVERED Final Report: 4-28-82-- 10-31-85
		6. PERFORMING ORG. REPORT NUMBER
7. AUTHOR(s) Daniel B. DeBra John Breakwell		8. CONTRACT OR GRANT NUMBER(s) F19628-82-K-0042
9. PERFORMING ORGANIZATION NAME AND ADDRESS Stanford University Guidance & Control Lab, Dept. of Aeronautics & Astronautics, Stanford, California 94305		10. PROGRAM ELEMENT, PROJECT, TASK AREA & WORK UNIT NUMBERS 63701B 320103AG
11. CONTROLLING OFFICE NAME AND ADDRESS Air Force Geophysics Laboratory Hanscom AFB, Massachusetts 01731 Contract Manager: Lt Terry Fundak/LWG		12. REPORT DATE February 1986
		13. NUMBER OF PAGES 40
14. MONITORING AGENCY NAME & ADDRESS (if different from Controlling Office)		15. SECURITY CLASS. (of this report) Unclassified
		15a. DECLASSIFICATION/DOWNGRADING SCHEDULE n/a
16. DISTRIBUTION STATEMENT (of this Report) APPROVED FOR PUBLIC RELEASE; DISTRIBUTION UNLIMITED		
17. DISTRIBUTION STATEMENT (of the abstract entered in Block 20, if different from Report) APPROVED FOR PUBLIC RELEASE; DISTRIBUTION UNLIMITED		
18. SUPPLEMENTARY NOTES Not applicable		
19. KEY WORDS (Continue on reverse side if necessary and identify by block number) gravity gradiometer, gravitational mass sensor, gravity mapping, mass attraction gradient, airborne gradiometer, inertial guidance, navigation, MASCONS		
20. ABSTRACT (Continue on reverse side if necessary and identify by block number) Gravity mapping requires a form for storing the data about the gravity field as well as an ability to make measurements and interpret them. The studies at Stanford University have included comparisons of gravity field models as well as some of the concerns associated with gathering data. Our earliest work included modeling of gravity gradiometer instruments in an attempt to correct for instrumental errors and reduce the residual measurement errors before doing gravity fitting. More recent work has been concerned with the errors introduced by mass attraction (OVER)		

DD FORM 1 JAN 73 1473

EDITION OF 1 NOV 65 IS OBSOLETE

S N 0102-LF-014-6601

Unclassified

SECURITY CLASSIFICATION OF THIS PAGE (When Data Entered)

Unclassified

SECURITY CLASSIFICATION OF THIS PAGE (When Data Entered)

Continuation of Block 20:

gradient of the vehicle carrying a gradiometer while data gathering and the proper patterns to use to maximize the separation of uncertainties in the gravity field from measurement noise.

S. N. 0102- LF- 014- 6601

SECURITY CLASSIFICATION OF THIS PAGE (When Data Entered)

TABLE OF CONTENTS

Introduction	1
Mascon Approximations	5
Introduction	5
The 2-Layer Mascon Model	6
Error Analysis	9
Numerical Results	12
Mascons With Improved Averaging	17
References	19
Appendix A	21
Efficient Gravity Gradient Data Gathering	25
Introduction	26
Models	26
Spectral Characteristics of the Field	26
Gravity Survey	28
Criteria for Comparison	29
Theory	29
Numerical Results	32
References	36



Special

INTRODUCTION

Most of our results have been documented in detail in the individual progress and annual reports. Our research and activities have included direct studies in support of gravity gradiometer survey missions as well as participation in related activities in which gravity mapping, instrument development work, reviews of gravity gradient programs and technical conferences involving the development of gravity gathering equipments, and reviews of states of the art. Indirectly related instrumental work in gravity gradiometry has included cryogenic gravity gradiometer development supported from AFOSR and jointly funded with our Physics Department. This class of instrument and its related technology is a candidate both for future gradiometers for survey work in aircraft and/or in orbit as well as for future, more accurate navigation requirements. We have benefited from studies we have performed for Goddard Space

Flight Center and the Johns Hopkins Applied Physics Laboratory in connection with GRAVSAT and gradiometers for orbital measurements. In addition to our direct support for their work, we have participated on planning groups and chaired a workshop at Goddard reviewing the technologies, both room temperature and low temperature, for orbital gravity gradiometry. We have participated in a review of the National Academy of Engineering of Precise Navigation for the Navy. Included in this advisory function was a study of the use of low-temperature technology for future Navy needs. Gravity gradiometers played an important role in all future navigation system considerations. In addition, we participated in some internal DOD reviews of technology strategies to ensure the best possible results for investment in development in gradiometry.

There are a variety of issues associated with data gathering and fitting gravity fields which have been studied. The aliasing due to spacing between ground tracks is a subject appropriate both for satellite data gathering as well as low altitude mapping missions. The local weighting of GRAVSAT doppler data in estimating surface gravity anomalies and undulations were reported on. The methods employed have application to other gravity gathering missions. An important step in changing the methods of estimating accuracy of gravity model fitting was made by inverting the classical problem. Typically, earlier studies were done by doing sensitivity analyses. Varying a parameter such as a spherical harmonic coefficient of the gravity field and looking at the effect on a measurement determined that there would be adequate sensitivity if a response was larger than the noise. However, many parameters

exist in the gravity field and this does not indicate whether they can be separated or not. A study on estimating accuracy of gravity gradient survey systems developed a theory of two-dimensional Fourier representation which changed the problem to the more direct estimation theory. Here one can answer questions of observability and determine directly the accuracy with which one could expect each of the parameters to be measured.

A variety of parameterizations are possible with gravity fields. Classically, spherical harmonic expansions have been used because the expansions involve orthogonal functions. The advantage here is that one can truncate such theories and know that the remaining functions represent the best fit. By contrast, the spherical harmonic expansion involves the gravity around the entire sphere. For much of the current interest in gravity, small patches must be modeled. For high resolution, the number of parameters needed becomes excessive when a world wide parameterization is used. One solution to this is to use mass concentrations and the number, size, and location of masses then become the parameters with which one works. Locally the size and variety is intense whereas at greater distances they can be sparse and still provide the resolution desired. An earlier report, "MASCON APPROXIMATIONS," has been revised during the past year (August 1985) and is included as an enclosure with this report.

Designing a gravity survey can have a significant influence both on the cost and the accuracy of the resulting model. Many investigators have made contributions in terms of spacing and the proper utilization

of data gathered in order to make the numerical data reduction techniques efficient. During the closing portions of this contract, we have addressed the question of the pattern that would provide the best opportunity to separate instrument noise from uncertainties in the gravity field. If one takes an orthogonal set of tracks and keeps that pattern constant, the question arises whether the order in which the tracks are traced would make a difference in the separability of instrument noise from the gravity uncertainties. Track crossings are when the measurements from the instrument should be the same along each path. The conjecture was that it would since the crossings occur with a different distribution in time. Thus, a pattern in which no crossings occurred until late in the survey would leave no check points during the first half of the survey, for example. By contrast, skipping paths would allow one to get the first crossing much earlier and distribute the crossings more uniformly throughout the survey. A theory was developed to evaluate the relative expected values of error and some numerical examples were calculated to indicate the promise or lack thereof of success. Unfortunately, the results do not indicate the improvement would be significant. This theoretical development and the numerical examples have been prepared in a paper which will be presented at the Air Force Academy on February 11, 1986. A copy of the paper is enclosed as a portion of this report.

MASCON APPROXIMATIONS

by

*John V. Breakwell
Department of
Aeronautics/Astronautics
Stanford University
Stanford, CA 94305*

*Weilian Yang
Chinese Academy of
Space Technology
Beijing
Peoples Republic of China*

1. INTRODUCTION

The error in representing the earth's gravity field by a large but finite number of mascons is clearly concentrated in the short wavelength part of the gravity spectrum. It is thus appropriate to use "flat-earth" approximations, as in [1], to estimate this error.

The most appropriate thin layers in which to locate the mascons are the idealized oblate spheroidal surface and the Haddon-Bullen layer 15 km below the surface, at the bottom of the earth's crust. Assuming that, as in [2], the earth density follows Jeffreys' model of regional isostatic compensation, the surface density fluctuations, confined to these two layers, can be estimated as in [1] from data of various sorts obtained from low satellites in polar orbit. Assuming a grid of mascons in each layer with separation Δ both NS and EW, the mass of a typical mascon may be chosen as the estimate of the integral of the surface density over a square of side Δ centered at the mascon grid point.

It is shown in this paper how to calculate the two-dimensional spectrum of the additional error in such quantities as the vertical and horizontal gravity components at satellite altitude z due to the finite separation Δ of the mascons.

Numerical results are presented for the case where the density fluctuations are estimated from gradiometer measurements taken in a low satellite, evaluated for various ratios Δ/z .

2. THE 2-LAYER MASCON MODEL

According to Jeffrey's dynamical model, the disturbing potential can be expressed as

$$\begin{aligned}
 u(x,y,z) = & \gamma \int_{-\infty}^{\infty} \int_{-\infty}^{\infty} \frac{\rho_1(u,v) du dv}{[(x-u)^2 + (y-v)^2 + z^2]^{1/2}} \\
 & + \gamma \int_{-\infty}^{\infty} \int_{-\infty}^{\infty} \frac{\rho_2(u,v) du dv}{[(x-u)^2 + (y-v)^2 + (z+H)^2]^{1/2}}
 \end{aligned} \tag{2.1}$$

where $\rho_1(u,v)$ is the surface-density fluctuation of the surface of the earth and $\rho_2(u,v)$ is the surface-density fluctuation of a compensating layer at depth $H = 15 \text{ km}$ [2]. γ is the universal gravitation constant. The relation between $\rho_1(u,v)$ and $\rho_2(u,v)$ is

$$d^4 \left[\left(\frac{\partial^2}{\partial u^2} + \frac{\partial^2}{\partial v^2} \right)^2 + 1 \right] \rho_2(u,v) = - \rho_1(u,v) \quad , \tag{2.2}$$

where $d = 48.1 \text{ km}$ in accordance with the Haddon-Bullen earth model, (2.1) can be rewritten as

$$u(x, y, z) = \gamma \sum_{n=-\infty}^{\infty} \sum_{m=-\infty}^{\infty} \iint_{D_{nm}} \frac{\rho_1(u, v) du dv}{[(x-u)^2 + (y-v)^2 + z^2]^{1/2}} \quad (2.3)$$

$$+ \gamma \sum_{n=-\infty}^{\infty} \sum_{m=-\infty}^{\infty} \iint_{D_{nm}} \frac{\rho_2(u, v) du dv}{[(x-u)^2 + (y-v)^2 + (z+H)^2]^{1/2}}$$

where the integral areas D_{nm} are defined as

$$D_{nm} = \{(x, y) | (n - 1/2)\Delta x \leq x < (n + 1/2)\Delta x, (m - 1/2)\Delta y \leq y < (m + 1/2)\Delta y\} \quad (2.4)$$

If $\Delta x, \Delta y$ are small enough, we can approximate

$$\iint_{D_{nm}} \frac{\rho_1(u, v) du dv}{[(x-u)^2 + (y-v)^2 + z^2]^{1/2}}$$

by

$$\frac{M_{nm}^{(1)}}{\{[x - n\Delta x]^2 + [y - m\Delta y]^2 + z^2\}^{1/2}},$$

and

$$\iint_{D_{nm}} \frac{\rho_2(u, v) du dv}{[(x-u)^2 + (y-v)^2 + (z+H)^2]^{1/2}}$$

by

$$\frac{M_{nm}^{(2)}}{\{[x - n\Delta x]^2 + [y - m\Delta y]^2 + (z + H)^2\}^{1/2}}, \quad (2.5)$$

and obtain the potential $u^t(x, y, z)$ of the 2-layer *mascon model*:

$$u^t(x, y, z) = \gamma \sum_{i=1}^2 \sum_{n=-\infty}^{\infty} \sum_{m=-\infty}^{\infty} \frac{M_{nm}^{(i)}}{[(x - n\Delta x)^2 + (y - m\Delta y)^2 + (z + H_i)^2]^{1/2}} \quad (2.6)$$

where $H_1 = 0$, $H_2 = H$. The simplest choice of $M_{nm}^{(i)}$ is $\Delta x \Delta y (\hat{\rho}_{AV}^{(i)})_{nm}$, where $(\hat{\rho}_{AV}^{(i)})_{nm}$ is the estimate, from satellite tracking or otherwise, of the average over D_{nm} of surface density ρ_i . We shall be mainly concerned in this paper with this definition of $M_{nm}^{(i)}$, but in the final section we shall look at more general definitions of average density.

We may express $u(x, y, z)$ and $u^*(x, y, z)$ as two-dimensional convolutions:

$$u(x, y, z) = \sum_{i=1}^2 \frac{\gamma}{\sqrt{x^2 + y^2 + (z + H_i)^2}} \otimes \rho_i(x, y) \quad (2.7)$$

and

$$u^*(x, y, z) = \sum_{i=1}^2 \frac{\gamma}{\sqrt{x^2 + y^2 + (z + H_i)^2}} \otimes [\tilde{\rho}_i(x, y) D(x, y)] \quad (2.8)$$

where $\tilde{\rho}_i(x, y)$ denotes the estimate of the average density in layer i over a rectangle with center (x, y) and dimension $\Delta x \cdot \Delta y$, and $D(x, y)$ denotes the periodic function:

$$D(x, y) = \Delta x \Delta y \sum_{n=-\infty}^{\infty} \sum_{m=-\infty}^{\infty} \delta(x - n\Delta x) \delta(y - m\Delta y) \quad (2.9)$$

with period Δx in x and period Δy in y .

This periodic function is easily found to have the Fourier series representation:

$$D(x, y) \sim \sum_{n=-\infty}^{\infty} \sum_{m=-\infty}^{\infty} e^{2\pi j \left(\frac{nx}{\Delta x} + \frac{my}{\Delta y} \right)} \quad (2.10)$$

3. ERROR ANALYSIS

Assume that $\rho_i(x, y)$ ($i = 1, 2$) are stationary random processes. Using two-dimensional Fourier transformation as in reference [1], (2.7) becomes

$$U(\vec{\omega}, z) = \frac{2\pi\gamma}{\omega} e^{-z\omega} [\rho_1(\vec{\omega}) + e^{-H\omega} \rho_2(\vec{\omega})] , \quad (3.1)$$

where $\vec{\omega} = \begin{pmatrix} \omega_x \\ \omega_y \end{pmatrix}$, $\omega = \sqrt{\omega_x^2 + \omega_y^2}$ and $\rho_i(\vec{\omega})$ denotes

$$\int_{-\infty}^{\infty} \int_{-\infty}^{\infty} \rho_i(x, y) e^{-j(\omega_x x + \omega_y y)} dx dy .$$

The dynamic compensating relation (2.2) becomes:

$$\rho_2(\vec{\omega}) = \frac{-\rho_1(\vec{\omega})}{1 + d^4 \omega^4} . \quad (3.2)$$

Combining (3.1), with $z = 0$, and (3.2), we obtain

$$\rho_i(\vec{\omega}) = C_i(\vec{\omega}) U_0(\vec{\omega}) , \quad (3.3)$$

where $U_0(\vec{\omega})$ denotes $U(\vec{\omega}, 0)$, and

$$C_1(\vec{\omega}) = \frac{\omega}{2\pi\gamma \left[1 - \frac{e^{-H\omega}}{1 + d^4 \omega^4} \right]} \quad (3.4)$$

$$C_2(\vec{\omega}) = \frac{\omega}{2\pi\gamma [e^{-H\omega} - (1 + d^4 \omega^4)]} .$$

The mascon model potential becomes:

$$U^{\dagger}(\vec{\omega}, z) = \frac{2\pi\gamma}{\omega} e^{-z\omega} [\rho_1^{\dagger}(\vec{\omega}) + e^{-H\omega} \rho_2^{\dagger}(\vec{\omega})] , \quad (3.5)$$

where $\rho_i^{\dagger}(\bar{\omega})$ denotes the Fourier transform of $[\tilde{\rho}_i(x,y)D(x,y)]$, expressible because of (2.10) as

$$\rho_i^{\dagger}(\bar{\omega}) = \sum_{n=-\infty}^{\infty} \sum_{m=-\infty}^{\infty} \tilde{\rho}_i(\bar{\omega} - \bar{\omega}_{nm}) , \quad (3.6)$$

where

$$\bar{\omega}_{nm} = \begin{pmatrix} \frac{2n\pi}{\Delta x} \\ \frac{2m\pi}{\Delta y} \end{pmatrix} . \quad (3.7)$$

The aliasing of $\tilde{\rho}_i$ in (3.6) is due to the finite mascon grid size.

In general, some gravity-related quantity $\eta(\bar{\omega})$, in which we are interested, can be expressed as

$$\eta(\bar{\omega}) = f_1(\bar{\omega})\rho_1(\bar{\omega}) + f_2(\bar{\omega})\rho_2(\bar{\omega}) \quad (3.8)$$

or, using matrix notation,

$$\eta(\bar{\omega}) = f^T(\bar{\omega})\rho(\bar{\omega}) , \quad (3.9)$$

where

$$f(\bar{\omega}) = \begin{pmatrix} f_1(\bar{\omega}) \\ f_2(\bar{\omega}) \end{pmatrix} , \quad \rho(\bar{\omega}) = \begin{pmatrix} \rho_1(\bar{\omega}) \\ \rho_2(\bar{\omega}) \end{pmatrix} . \quad (3.10)$$

And the approximation $\eta^{\dagger}(\bar{\omega})$, of $\eta(\bar{\omega})$ in the mascon model is given by

$$\eta^{\dagger}(\bar{\omega}) = f^T(\bar{\omega}) \sum_{n=-\infty}^{\infty} \sum_{m=-\infty}^{\infty} \tilde{\rho}(\bar{\omega} - \bar{\omega}_{nm}) . \quad (3.11)$$

The next step is to analyze the error $\Delta\eta$ caused by using the mascon

model, where

$$\Delta\eta(\vec{\omega}) = \eta^{\dagger}(\vec{\omega}) - \eta(\vec{\omega}) \quad (3.12)$$

Firstly, the average ρ over a typical rectangle has Fourier Transform:

$$\rho_{AV}(\vec{\omega}) = B(\vec{\omega})\rho(\vec{\omega}) \quad (3.13)$$

where, in the case of simple averaging, B is the scalar:

$$B(\vec{\omega}) = \frac{4\sin\left(\frac{\omega_x\Delta x}{2}\right)\sin\left(\frac{\omega_y\Delta y}{2}\right)}{\omega_x\omega_y\Delta x\Delta y} \quad (3.14)$$

Next, assuming measurements:

$$\varsigma(\vec{\omega}) = H(\vec{\omega})U_0(\vec{\omega}) + W, \quad (3.15)$$

where W is a white-noise measurement error, the best estimate $\tilde{\rho}$ of ρ_{AV} is given, as in reference [1], by

$$\tilde{\rho} = \psi^T(\vec{\omega})\varsigma(\vec{\omega}), \quad (3.16)$$

where

$$\psi(\vec{\omega}) = \frac{\Phi_W^{-1}H(-\vec{\omega})\phi_{U_0}(\vec{\omega})C^T(\vec{\omega})B^T(\vec{\omega})}{1 + \phi_{U_0}(\vec{\omega})H^T(\vec{\omega})\Phi_W^{-1}H(-\vec{\omega})}, \quad (3.17)$$

and Φ_W and ϕ_{U_0} are the spectral densities of the measurement error and the disturbing potential at the earth's surface.

Combining (3.9), (3.11), (3.12), (3.15), (3.16) and (3.17) we can deduce the spectral density of the error $\Delta\eta$. After some simplification (see Appendix A) this

is:

$$\begin{aligned} \phi_{\Delta\eta}(\omega) = & \frac{f^T(-\omega)C(-\omega)\phi_{U_0}(\omega)C^T(\omega)f(\omega)}{1 + \phi_{U_0}(\omega)H^T(\omega)\Phi_W^{-1}H(\omega)} \\ & + \frac{\phi_{U_0}(\omega)H^T(\omega)\Phi_W^{-1}H(\omega)}{1 + \phi_{U_0}(\omega)H^T(\omega)\Phi_W^{-1}H(\omega)} \left\{ \sum'_{m,n} f^T(\omega_{nm}-\omega)B(-\omega)C(-\omega)\phi_{U_0}(\omega) \right. \\ & \cdot \left. C^T(\omega)B^T(\omega)f(\omega-\omega_{nm}) + f^T(-\omega)[B(-\omega)-I]C(-\omega)\phi_{U_0}(\omega)C^T(\omega)[B^T(\omega)-I]f(\omega) \right\}, \end{aligned} \quad (3.18)$$

where $\sum'_{m,n}$ denotes $\sum_{m \neq 0 \text{ or } n \neq 0} \sum_n$, and I denotes the identity matrix.

The first term on the righthand side of (3.25) is the spectrum of the error in estimating η due to measurement errors without any mascon approximation. The terms in parentheses $\{ \}$ in the second term on the righthand side of (3.25) constitute the error in η due to the mascon approximation, assuming perfect measurements. The factor in front of the parentheses is the ratio (signal)/(signal + noise), and attenuates at high frequency.

4. NUMERICAL RESULTS

The quantity η of interest is taken to be the vertical gravity anomaly $g(z)$ at satellite altitude z . Thus, as in reference [1], the scalar $C^T(\omega)f(\omega)$ is just $\omega e^{-\omega z}$, where $\omega = |\omega| = \sqrt{\omega_x^2 + \omega_y^2}$. The $NS(x)$ and $EW(y)$ spacings are assumed equal: $\Delta x = \Delta y = \Delta$. The estimation of average densities is assumed

to be based on vertical gradiometer measurements in a polar satellite at the altitude $z = 180 \text{ km}$. Thus, as in reference [1], $H(\omega)$ is the scalar $\omega^2 e^{-\omega z}$. Independent gradiometer measurements are assumed to be available every 8 sec for 6 months with an accuracy σ_W of either 0.1 Eotvos or 0.01 Eotvos, so that $\Phi_W = 2\pi^2 R^2 \sigma_W^2 / N$, with $N \cong 1.92 \times 10^6$, $R(\text{km}) = \text{earth radius}$ and $\sigma_W = 10^{-10} \text{ sec}^{-2}$ or $10^{-11} \text{ sec}^{-2}$. The spectrum ϕ_{U_0} of the surface disturbing potential is obtained, as in reference [1], from the top 3 layers of a model due to Heller containing 5 layers of fictitious white-noise potential. The constructed mascon model is assumed to be superimposed on a low-order potential coefficient model up to degree $l_0 = 10$. The mean squared $\Delta\eta$ is thus obtained, as in reference [1], by integrating $(1/4\pi^2)$ times $\phi_{\Delta\eta}(\omega)$, in (3.25), over the region $\omega \geq l_0/R$.

Table 1 corresponds to the integral of the first term in (3.25), while Tables 2a and 2b correspond to the integral of the second term. The effect of σ_W in Tables 2 was not noticeable since the factor (signal)/(signal + noise) was essentially unity over the dominant frequency range.

Comparison of Tables 1 and 2a suggest that the ratio Δ/z need not be chosen less than 0.5 if σ_W is 0.1 Eotvos, or not much less than 0.2 if σ_W is 0.01 Eotvos. However, in practice, a potential coefficient model is truncated at some maximum degree l_1 and the consequent truncation error will often dominate the estimation error in Table 1. The $\sigma_{\Delta g(z)}^2$ from truncation is the integral of $(1/4\pi^2)$ times $(\omega^2 e^{-2\omega z} \phi_{U_0}(\omega))$ over the region $\omega \geq l_1/R$. The corresponding

Table 1 $\sigma_{\Delta g(z)}$ (m gal) From Estimation Error

	180	240	300
0.1E	0.19	0.15	0.14
0.01E	0.022	0.018	0.017

Table 2a $\sigma_{\Delta g(z)}$ (m gal) From Mascon Model Error

	180	240	300
0.2	0.027	0.027	0.027
0.25	0.044	0.041	0.037
0.33	0.077	0.068	0.062
0.5	0.16	0.15	0.15

Table 2b $\sigma_{\Delta g(z)}$ (m gal) From Mascon Model Error

	180	240	300
110	0.23	0.12	0.075
165	0.76	0.33	0.20
220	2.1	0.71	0.38

Table 3 $\sigma_{\Delta g(z)}$ (m gal) From Truncation

	180	240	300
180	.043	.0069	.0011
135	.19	.048	.012
90	.78	.28	.11

$\sigma_{\Delta g(z)}$ is shown in Table 3.

Comparison of Tables 2b and 3 suggests, for example, that a mascon model with $\Delta = 165 \text{ km}$ will yield about the same accuracy (.78 mgal) at $z = 180 \text{ km}$ as a potential coefficient model truncated at degree $l_1 = 90$. Since the number of potential coefficients $\sim l_1^2 = 8,100$, while the number of mascons in 2 layers $\sim 2 \times 4\pi R^2/\Delta^2 \sim 37,470$, the mascon model would appear to be less efficient by a factor 4. However it is evident that in computing $g(z)$ at a particular position in orbit the mascons located at a distance greater than r_{MAX} from the subsatellite point can be omitted if r_{MAX} is sufficiently large, without appreciable degradation in accuracy. To give a quantitative answer to the approximate choice of r_{MAX} it would be necessary to take into account the cross-correlation of the mascons. This would lead to a quadruple integral for the spectrum of the additional error and a sextuple integral for the mean-squared additional error itself!

A crude criterion for the choice of r_{MAX} is obtainable if we pretend that the mascons are statistically independent. Since the vertical gravity due to a mascon m_{ij} at relative horizontal position \bar{r}_{ij} contains the factor $z/(z^2 + r_{ij}^2)^{3/2}$, the additional error due to omission of mascons with $r_{ij} > r_{MAX}$ is given by:

Table 4 $\sigma_{\Delta g(z)}$ (*m gal*) From Mascon Model Error
With Optimal Scalar Averaging

	180	240	300
110	.050	.0080	.0013
165	.39	.11	.031
220	1.10	.37	.14

Table 5 $\sigma_{\Delta g(z)}$ (*m gal*) From Mascon Model Error
With Optimal Matrix Averaging

	180	240	300
110	.0088	.00068	.000052
165	.13	.024	.0045
220	.42	.12	.034

$$\sigma_{\Delta g(z)}^2 / \sigma_{g(z)}^2 = \int_{r_{MAX}}^{\infty} rz^2(z^2+r^2)^{-3} dr / \int_0^{\infty} rz^2(z^2+r^2)^{-3} dr$$

$$= (1 + r_{MAX}^2/z^2)^{-2} ,$$

where $\sigma_{g(z)}^2$ is the *a priori* variance of $g(z)$. Since $\sigma_{g(z)} \sim 9 \text{ mgal}$ at $z = 180 \text{ km}$, we can obtain $\sigma_{\Delta g(z)} \sim 0.55 \text{ mgal}$ by choosing $r_{MAX} = 3.9z$. With the spacing $\Delta = 150 \text{ km}$, we need only about 138 *local* mascons to achieve a total error of about 0.78 mgal , equivalent to that obtained from the potential coefficient model with 8,100 terms.

5. MASCONS WITH IMPROVED AVERAGING

Instead of the scalar averaging operator $B(\overline{\omega})$ of (3.21) corresponding to uniform averaging over the typical rectangle, it is possible to choose $B(\overline{\omega})$ so as to minimize the second term in (3.25). This can be carried out either by restricting $B(\overline{\omega})$ in (3.20) to be a scalar, or by allowing $B(\overline{\omega})$ to be a 2×2 matrix. In either case, the averaging suffers from the disadvantage of being dependent on $f(\overline{\omega})$; i.e. in either case the computed mascons would depend on satellite altitude z . On the other hand, the improvements over simple averaging are surprising. Table 4 shows the mascon model error with optimal scalar averaging in (3.20), and Table 5 shows the results for optimal matrix averaging. The improvement in Table 5 over Table 4 is presumably due to taking better advantage of Jeffreys' dynamic compensation.

REFERENCES

- [1] Breakwell, John, V., "Satellite Determination of Short Wavelength Gravity Variations," *J. Astronaut. Sci.*, Vol. XXVII, No. 4, 1979.
- [2] Jordan, Stanley K., "Statistical Models for Gravity, Topography and Density Contrasts in the Earth," *J. Geophys. Res.*, Vol. 83, April 10, 1978.

APPENDIX A

Firstly, the error $\Delta\eta(\vec{r})$ like $\eta^{\dagger}(\vec{r})$ is no longer a stationary two-dimensional process. Its autocorrelation function $\phi_{\Delta\eta}(\vec{r},\vec{\rho}) \triangleq E[\Delta\eta(\vec{r}),\Delta\eta(\vec{r}+\vec{\rho})]$, depends on the position \vec{r} relative to the local rectangle, as does also its Fourier Transform $\phi_{\Delta\eta}(\vec{r},\vec{\omega})$, the error spectral density. But we shall subsequently average over \vec{r} .

Now $\phi_{\Delta\eta}$ is expressible as

$$\phi_{\Delta\eta} = \phi_{\eta^{\dagger}\eta^{\dagger}} - \phi_{\eta^{\dagger}\eta} - \phi_{\eta\eta^{\dagger}} + \phi_{\eta\eta} \quad , \quad (\text{A.1})$$

where

$$\phi_{\eta^{\dagger}\eta} = \frac{1}{4\pi^2} \int_{-\infty}^{\infty} \int_{-\infty}^{\infty} e^{-j(\omega\xi + \omega_y\eta)} E\left[\left(\int_{-\infty}^{\infty} \int_{-\infty}^{\infty} f^T(x',y') \widetilde{\rho}(x-x',y-y') D(x-x',y-y') dx' dy'\right) \right. \\ \left. \left(\int_{-\infty}^{\infty} \int_{-\infty}^{\infty} \rho^T(x+\xi-x',y+\eta-y') f(x',y') dx' dy'\right) \right] d\xi d\eta \quad (\text{A.2})$$

and

$$E[\widetilde{\rho}(x-x',y-y') \rho^T(x+\xi-x',y+\eta-y')] = C_{\rho\rho}(\xi+x'-x',\eta+y'-y') \quad ,$$

so that, using (2.9) and introducing $\xi' = \xi+x'-x'$, $\eta' = \eta+y'-y'$:

$$\phi_{\eta^{\dagger}\eta} = \frac{1}{4\pi^2} \int_{-\infty}^{\infty} \int_{-\infty}^{\infty} \int_{-\infty}^{\infty} \int_{-\infty}^{\infty} e^{-j[\omega(\xi'-x'+x') + \omega_y(\eta'-y'+y')]} \sum_n \sum_m e^{2\pi j \left[\frac{n(x-x')}{\Delta x} + \frac{m(y-y')}{\Delta y} \right]}$$

$$f^T(x',y') C_{\rho\rho}(\xi',\eta') f(x',y') dx' dy' dx' dy' d\xi' d\eta'$$

Averaging over (x,y) removes all terms from the double sum except

$n = 0, m = 0$. Using the fact that

$$\phi_{\rho}^{\sim}(\omega) = \frac{1}{4\pi^2} \int_{-\infty}^{\infty} \int_{-\infty}^{\infty} e^{-j(\omega, \xi + \omega, \eta')} \widetilde{C}_{\rho}(\xi', \eta') d\xi' d\eta'$$

we are left with:

$$\phi_{\eta; \eta}(\omega) = f^T(-\omega) \phi_{\rho}^{\sim}(\omega) f(\omega) \quad (\text{A.3})$$

Similarly

$$\phi_{\eta \eta}(\omega) = f^T(-\omega) \phi_{\rho \rho}^{\sim}(\omega) f(\omega) \quad (\text{A.4})$$

Next

$$\begin{aligned} \phi_{\eta; \eta}(\omega) &= \frac{1}{4\pi^2} \int_{-\infty}^{\infty} \int_{-\infty}^{\infty} e^{-j(\omega, \xi + \omega, \eta)} E \left[\left(\int_{-\infty}^{\infty} \int_{-\infty}^{\infty} f^T(x', y') \widetilde{\rho}(x-x', y-y') \right. \right. \\ &\quad \cdot D(x-x', y-y') dx' dy' \left. \left(\int_{-\infty}^{\infty} \int_{-\infty}^{\infty} \rho^T(x+\xi-x', y+\eta-y') \right. \right. \\ &\quad \cdot D(x+\xi-x', y+\eta-y') f(x', y') dx' dy' \left. \right) d\xi d\eta \\ &= \frac{1}{4\pi^2} \int_{-\infty}^{\infty} \int_{-\infty}^{\infty} \int_{-\infty}^{\infty} \int_{-\infty}^{\infty} e^{-j(\omega, (\xi' - x' + x') + \omega, (\eta' - y' + y'))} \\ &\quad \sum_n \sum_m \sum_{n'} \sum_{m'} e^{2\pi j \left[\frac{n(x-x') + n'(x+\xi-x')}{\Delta x} + \frac{m(y-y') + m'(y+\eta-y')}{\Delta y} \right]} \end{aligned} \quad (\text{A.5})$$

$$f^T(x', y') \widetilde{C}_{\eta \eta}(\xi', \eta') f(x', y') dx' dy' dx' dy' d\xi' d\eta'$$

Averaging over (x, y) removes all terms from the quadruple sum except $n' = -n, m' = -m$. This leaves:

$$\phi_{\eta\eta}(\bar{\omega}) = \sum_n \sum_m f^T(-\bar{\omega}) \phi_{\rho\rho}(\bar{\omega} + \bar{\omega}_{nm}) f(\bar{\omega}) \quad (\text{A.6})$$

Furthermore, from (3.3), (3.15) and (3.16):

$$\phi_{\rho\rho}(\bar{\omega}) = \psi^T(-\bar{\omega}) H(-\bar{\omega}) \phi_{U_0}(\bar{\omega}) C^T(\bar{\omega}) \quad (\text{A.7})$$

$$\phi_{\rho\rho}(\bar{\omega}) = C(-\bar{\omega}) \phi_{U_0}(\bar{\omega}) H^T(\bar{\omega}) \psi(\bar{\omega})$$

and

$$\phi_{\rho\rho}(\bar{\omega}) = \psi^T(-\bar{\omega}) [H(-\bar{\omega}) \phi_{U_0}(\bar{\omega}) H^T(\bar{\omega}) + \Phi_W] \psi(\bar{\omega}) \quad (\text{A.8})$$

Substitution into (A.1) yields

$$\phi_{\Delta\eta}(\bar{\omega}) = \sum_{m,n} f^T(-\bar{\omega}) \psi^T(-\bar{\omega} + \bar{\omega}_{nm}) [H(-\bar{\omega} + \bar{\omega}_{nm}) \phi_{U_0}(\bar{\omega} - \bar{\omega}_{nm}) H^T(\bar{\omega} - \bar{\omega}_{nm}) + \Phi_W]$$

$$\psi(\bar{\omega} - \bar{\omega}_{nm}) f(\bar{\omega}) - f^T(-\bar{\omega}) C(-\bar{\omega}) \phi_{U_0}(\bar{\omega}) H^T(\bar{\omega}) \psi(\bar{\omega}) f(\bar{\omega})$$

$$- f^T(-\bar{\omega}) \psi^T(-\bar{\omega}) H(-\bar{\omega}) \phi_{U_0}(\bar{\omega}) C^T(\bar{\omega}) f(\bar{\omega}) + f^T(-\bar{\omega}) C(-\bar{\omega}) \phi_{U_0}(\bar{\omega}) C(\bar{\omega}) f(\bar{\omega})$$

Since $\sigma_{\Delta\eta}^2$ will be obtained as $\frac{1}{4\pi^2} \iint \phi_{\Delta\eta}(\bar{\omega}) d\omega_x d\omega_y$, it is permissible to replace

$\bar{\omega} + \bar{\omega}_{nm}$ by $\bar{\omega}$ and $\bar{\omega}$ by $\bar{\omega} - \bar{\omega}_{nm}$ in each term of the summation in the first term in $\phi_{\Delta\eta}$. Finally, substituting for $\psi(\bar{\omega})$ from (3.17), we obtain (3.18).

ABSTRACT

Efficient Gravity Gradient Data Gathering

M. Bilello, J. V. Breakwell, D. B. DeBra

We are interested in how one can separate the variations in a gravity field from the measurement noise when making a survey. Given a survey pattern in which the path of the instrument crosses itself (as it does in a series of orthogonal tracks), there are a discrete number of instants at which the measurements should be identical. We have examined a number of different sequences in generating the survey pattern to vary the times at which these identical conditions occur. The conjecture was that an appropriate choice of pattern could take advantage of the time characteristics of the measurement noise in permitting a separation of noise from gravity data. We show the results as a function of the correlation time of the measurement noise for a simple model of the gravity field. For noise varying from uncorrelated to a correlation time comparable to the survey time, the variation is approximately 10%. Large differences in accuracy of reconstruction do not appear likely since our results give variation between paths of approximately 2% for two very dissimilar paths through the same grid. Thus the conjecture has not been borne out.

Efficient Gravity Gradient Data Gathering

Introduction

The modern interest in measuring gravity gradients began in the late 1950s motivated by determining the vertical in a satellite. Early papers considering the analytical aspect of gradient determination were followed in the next decade by a number of innovative approaches in how such an instrument might be built. The revolution in gradiometry was to make the measurements in a moving vehicle and/or in a satellite without the gravity needed for the geophysical pendulum instruments. An instrument developed at the Bell Aerosystems was chosen for field application for improvements in navigation. This instrument has been very successful in its early field tests and is in production for deployment. As a result of this success for the navigation mission, the Defense Mapping Agency (DMA) through the Air Force Geophysics Laboratory (AFGL) began the modification of this instrument for gravity gradient measurements for gravity survey work. Many people have subsequently contributed to the development of a survey plan and techniques for utilisation of such an instrument. In this paper we explore the possibility that given an area to be surveyed and a track spacing that has been determined by the necessary resolution of gravity data, there might be improvements in accuracy depending upon the form of a grid pattern used in overflying the area. The conjecture is based on the fact that instrument noise, whether described in the time domain or spectrally, may be different than the equivalent noise associated with gravity fields for a given velocity of the vehicle during the survey. When a survey is performed with a grid in which tracks cross each other, there are a discrete number of crossings at which the measurements should be the same in both directions. Different patterns provide a different distribution in time of when these points of identical measurement occur. It is this variation in the distribution and time which could make a difference in being able to separate signal from noise.

Models

As indicated in the introduction, the spectral characteristics of the gravity field and of the instrument will have an influence on the separability of the gravity information from the instrument noise. With the amount of experimental data that exists from the laboratory and early field trials, it would be possible to give a good model of the expected noise from a gravity gradiometer. However, to investigate the potential for improvement one can start with a much simpler model of the instrument noise and vary its parameters to see whether or not significant improvements are possible. We have chosen the latter approach to investigate the feasibility of improvement with the expectation that if significant improvements appear possible we would then improve the model using available empirical data.

Spectral Characteristics of the Field

We have used a model of the gravity gradient field that allows us to determine the spatial correlations of the gravity gradient. (J.V. Breakwell [1]).

Using an approximation of flat earth, we can write:
 $U(\vec{\omega}, h) = e^{-h\omega} U(\vec{\omega}, 0)$ where $U(\vec{\omega}, 0)$ is the Fourier transform of $U(x, y, 0)$, potential on the reference surface of the earth and $U(\vec{\omega}, h)$, is the Fourier transform of $U(x, y, h)$, gravity potential at altitude h .

Then the gravity gradients components are given by:

$$\begin{bmatrix} U_{xx}(\vec{\omega}, h) \\ U_{yy}(\vec{\omega}, h) \\ U_{zz}(\vec{\omega}, h) \\ U_{xy}(\vec{\omega}, h) \\ U_{xz}(\vec{\omega}, h) \\ U_{yz}(\vec{\omega}, h) \end{bmatrix} = e^{-h\omega} \begin{bmatrix} -\omega_x^2 \\ -\omega_y^2 \\ \omega^2 \\ -\omega_x\omega_y \\ -j\omega_x\omega \\ -j\omega_y\omega \end{bmatrix} U(\vec{\omega}, 0) \quad (1)$$

where

$$\vec{\omega} = (\omega_x, \omega_y) \\ \omega = \sqrt{\omega_x^2 + \omega_y^2}$$

From Heller's model referenced in [1], we get the spectral density of $U(x, y, 0)$ with correlation distance D_i :

$$\phi_{U_0}(\vec{\omega}) = \phi_{U_0}(\omega) = \sum_{i=1}^3 \phi_i e^{-2\omega D_i}$$

Equation (1) can be viewed as a representation of a linear system with $U(\vec{\omega}, 0)$ as input and

$$H(j\omega) = e^{-h\omega} \begin{bmatrix} -\omega_x^2 \\ -\omega_y^2 \\ \omega^2 \\ -\omega_x\omega_y \\ -j\omega_x\omega \\ -j\omega_y\omega \end{bmatrix}$$

as the transfer function.

Then we can compute the spectral densities of the gravity gradient components at altitude h :

$$\phi_{U_0}(\vec{\omega}, h) = |H(j\omega)|^2 \phi_{U_0}(\vec{\omega})$$

$$\begin{bmatrix} \phi_{U_{xx}}(\vec{\omega}, h) \\ \phi_{U_{yy}}(\vec{\omega}, h) \\ \phi_{U_{zz}}(\vec{\omega}, h) \\ \phi_{U_{xy}}(\vec{\omega}, h) \\ \phi_{U_{xz}}(\vec{\omega}, h) \\ \phi_{U_{yz}}(\vec{\omega}, h) \end{bmatrix} = e^{-2\omega h} \begin{bmatrix} \omega_x^4 \\ \omega_y^4 \\ \omega^4 \\ \omega_x^2\omega_y^2 \\ \omega_x^3\omega \\ \omega_y^3\omega \end{bmatrix} \phi_{U_0}(\vec{\omega})$$

By taking the inverse Fourier transform, we can determine the auto-correlation functions for the gradients, say $S_U(x, y, h)$.

Example: Say we want to compute $S_{U_{..}}(x, y, h)$ we have

$$\phi_{U_{..}}(\vec{\omega}, h) = e^{-2\omega h} \omega^4 \phi_{U_{..}}(\omega) = \sum_{i=1}^3 \phi_i \omega^4 e^{-2\omega(h+D_i)}$$

then

$$S_{U_{..}}(x, y, h) = \sum_{i=1}^3 \phi_i \int \int_{-\infty}^{+\infty} e^{j(\omega_x x + \omega_y y)} \omega^4 e^{-2\omega(h+D_i)} d\omega_x d\omega_y$$

or

$$S_{U_{..}}(r, \theta, h) = \sum_{i=1}^3 \phi_i \int_0^{2\pi} \int_0^{+\infty} e^{j r \omega \cos(\theta - \alpha)} \omega^5 e^{-2\omega(h+D_i)} d\omega d\alpha$$

that is

$$S_{U_{..}}(r, h) = \sum_{i=1}^3 \phi_i 2\pi \int_0^{+\infty} \omega^5 e^{2\omega(h+D_i)} J_0(r\omega) d\omega$$

Where $J_0(r\omega)$ is a Bessel function of the first kind in $r\omega$, in the special case of a flight path over a point grid, we need to compute $S_p = E[s_p s_p^T]$, where s_p is the sequence of

signals we want to estimate $s_p = \begin{bmatrix} s_{p1} \\ \vdots \\ s_{pN} \end{bmatrix}$.

Let's suppose that we are measuring the component U_{zz} of the gradient, then:

$$E[s_p, s_p] = S_{U_{..}}(r_{ij}, h)$$

where

$$r_{ij} = \| \overrightarrow{P_i P_j} \|,$$

is the distance between points P_i and P_j .

Gravity Survey

To perform a gravity survey, the craft which carries the instruments follows a particular path. In the simple case of a square survey area, a possible strategy is to fly parallel tracks as shown in Figure 1.

However, in order to remove drifts and red noise from the measurements, a better way is to make cross checks, taking two measurements at two different times at the same point. The grid of Figure 2.1 is an example of this type of flight. Also shown is the time of second crossing, Figure 2.2., and the time between the two crossings versus the point

of interest, Figure 2.3. One can see that for the path of Figure 2.2, the crossings occur essentially during the second half of the total survey time T and that when they begin to occur, it is in such a way that they are close to each other in space.

In order to get a better time and space distribution of second crossings, a path such as the one shown in Figure 3.1 might be of interest. Here, a row or column is skipped at each pass, and the effect can be seen in Figures 3.2 and 3.3. Basically, second crossings occur earlier and two consecutive ones are more likely to be spread in time. Another advantage of this kind of path is the possibility to continue to make measurements while turning between two tracks. If one row or column (or more) is skipped, then the radius of curvature in the turning is bigger, so that both the bank angle and the induced acceleration are smaller. This may allow the instrument platform to remain in tolerable perturbations and compensations may be possible.

In view of the disappointing results that we are about to give, we did not pursue the question of efficiency due to variations in the radius of turns, nor did we carry the study to include the effect of mass attraction and error modeling on the instrument.

Criteria for Comparison

Our purpose is to get an estimate of the gravity gradient at the grid points with the smallest error-standard deviation. Since all points are a priori of equal importance, we take as the performance criterion the arithmetic mean of the standard deviation obtained at each point, that is:

$$\sigma_{per} = \frac{1}{N} \sum_{i=1}^N \sigma_i$$

where $\sigma_i = \sqrt{P_i}$ and P_i is the variance of the error in the gravity quantity at point i : $P_i \equiv E[(s_p - \hat{s}_p)^2]$. N is the number of points on the grid. Thus, we will be considering as the best path the one that minimises the criterion σ_{per} .

Theory

The gradiometer output signals consist of the sum of a signal to be estimated (gravity quantity) and the noise inherent in the instrument.

$y = s + n$ where s is any one of the gravity gradient components and n is the instrument noise. If we take M measurements at M different times, we have in vector form:

$$y = s + n \text{ where } y = \begin{bmatrix} y_1 \\ \vdots \\ y_M \end{bmatrix} s = \begin{bmatrix} s_1 \\ \vdots \\ s_M \end{bmatrix}; n = \begin{bmatrix} n_1 \\ \vdots \\ n_M \end{bmatrix}$$

where n_j is the instrument noise at time t_j , etc. ...

If the pattern is a square grid with intersecting points, then $M = 2p^2$ where p is the number of points on the side of the square grid.

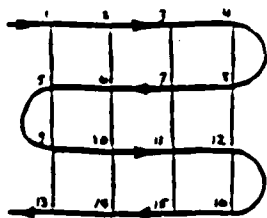


fig. 1

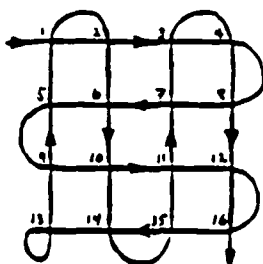


fig. 2.1

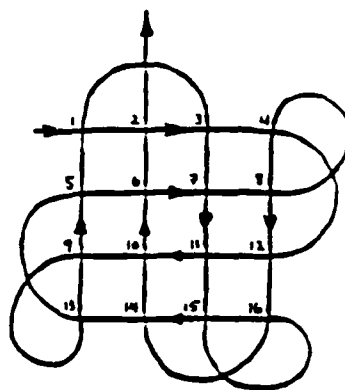


fig. 3.1

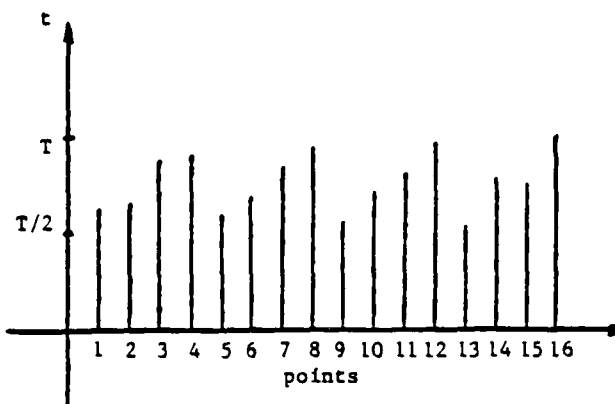


fig. 2.2

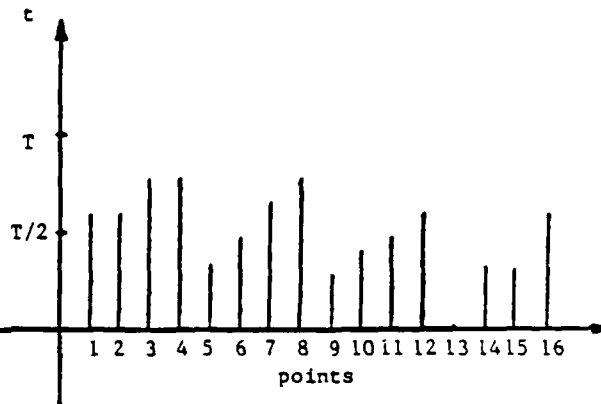


fig. 2.3

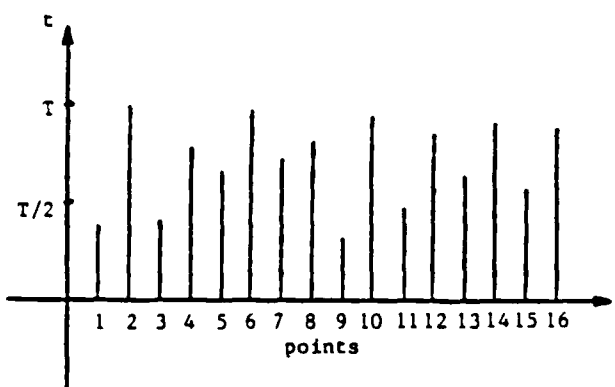


fig. 3.2

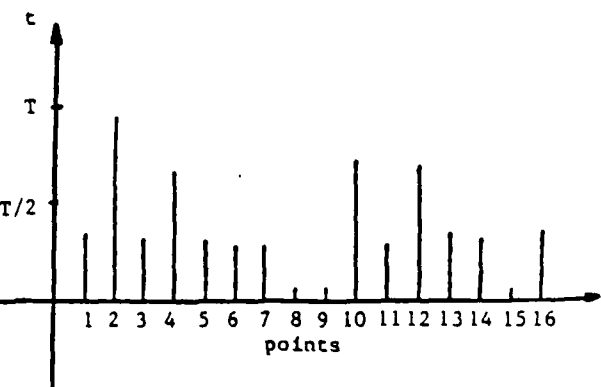


fig. 3.3

Figs.

The sketches above show 4 by 4 grids. The speed of the craft is uniform and the turning times are neglected. In Fig. 2.2 and 3.2, the time of the second crossing at each point (from 1 to 16) is plotted, while Figs. 2.3 and 3.3 show the time between the two crossings for each point (from 1 to 16).

We assume for simplicity a linear estimate from the observations:

$\hat{z} = Ky$ where K is an $M \times M$ gain matrix. This is a smoothing formula where we use all the collected data to estimate the gravity quantity at each point.

The error in the estimate is $\bar{s} \triangleq s - \hat{z}$ or $\bar{s} = (I - K)s - Kn$.

Then the covariance matrix of the error, say P , can be computed:

$$P = E[\bar{s}\bar{s}^T] = (I - K)S(I - K)^T + K N K^T - (I - K)E[sn^T]K^T - K E[ns^T](I - K^T)$$

where $S \triangleq E[ss^T]$ and $N \triangleq E[nn^T]$.

The gravity signal s and the instrument noise being uncorrelated, the formula reduces to:

$$P = (I - K)S(I - K)^T + K N K^T$$

Then we choose the gain matrix K that minimises the trace of P (least squares estimate) that is:

$$d(\text{tr}(P)) = \text{tr}[(-(I - K)S + KN)dK^T + dK(-S(I - K)^T + NK^T)] = 0$$

This yields $-(I - K)S + KN = 0$ or $K = S(S + N)^{-1}$ whenever the inverse exists and in this case K exists and is unique. We remark that if $(S + N)$ is non invertible then $E[yy^T]$ is non invertible. Minimising every term P_{ii} leads to the same gain matrix K . The linear least squares estimate is then deduced $\hat{z} = S(S + N)^{-1}y$. The performance of the estimate is judged upon the error covariance matrix and more precisely on the diagonal entries of this matrix. Substituting for K in the expression of P , we get:

$$P = S(S + N)^{-1}N$$

In addition to the fact that n and s are uncorrelated, we have implicitly assumed that s and n are zero-mean signals. If this is not the case, ($E(s) \neq 0$ and/or $E(n) \neq 0$ but still $E[ns^T] = E[sn^T] = 0$), then the formulae are modified in such a way that we replace the random variables with their centered counterparts, namely:

where ($y = s + n$)

$$\begin{cases} \hat{z} = E(s) + K(y - E(y)) \\ K = S^*(S^* + N^*)^{-1} \\ P = S^*(S^* + N^*)^{-1}N^* \end{cases}$$

with

$$S^* \triangleq E[ss^T] - E[s]E[s^T]$$

$$N \triangleq E[nn^T] - E[n]E[n^T]$$

Then for a particular pattern that links times to points, we associate the variance $P(t_j, t_j)$ with the point which is flown over at time t_j .

However, for a grid with crossed points, it turns out that it is never necessary to take the inverse of the $M \times M$ matrix $(S + N)$ because as can be expected, there are a lot of redundancies in the matrix P computed as $P = S(S + N)^{-1}N$. For example, if at times j and k the same point is flown over (with $j \neq k$), then obviously $P(t_j, t_i) = P(t_k, t_i) \forall i$; in particular, $P(t_j, t_j) = P(t_k, t_k)$.

We detail this in the next section on preliminary numerical results.

Numerical Results

We take for our example $p = 4$ and there are $16 = p^2$ points on the grid and we show first how to reduce the size of the matrix to be inverted $(S + N)$ (the path lasts M units of time).

Let

$$s_t = \begin{bmatrix} s_{t_1} \\ \vdots \\ s_{t_M} \end{bmatrix} \quad \text{and} \quad s_p = \begin{bmatrix} s_{p_1} \\ \vdots \\ s_{p_N} \end{bmatrix} \quad \text{also} \quad n_t = \begin{bmatrix} n_{t_1} \\ \vdots \\ n_{t_M} \end{bmatrix} \quad n_p = \begin{bmatrix} n_{p_1} \\ \vdots \\ n_{p_N} \end{bmatrix}$$

where the subscripts t stand for time and p for points ($N = p^2$)

then

$$\begin{cases} s_t = F s_p \\ n_t = F n_p \end{cases}$$

where F is the $M \times p^2$ matrix that maps the points to the times, i.e., $F(i, j) = 1$ if point j is flown over at time i , and 0 otherwise.

F is full rank and let F_i be the pseudo-inverse of F (F_i is $p^2 \times M$) then we can write

$$\begin{cases} S_t = F S_p F^T \\ N_t = F N_p F^T \end{cases} \quad \begin{cases} S_p = F_i S_t F_i^T \\ N_p = F_i N_t F_i^T \end{cases}$$

where

$$S = E[ss^T]$$

$$N = E[nn^T]$$

From previous results we had:

$$P_t = S_t(S_t + N_t)^{-1}N_t$$

which yields

$$P_i = F S_p F^T [F S_p F^T + F N_p F^T]^{-1} F N_p F^T$$

or

$$P_i = F S_p F^T [F (S_p + N_p) F^T]^{-1} F N_p F^T$$

but

$$F^T [F (S_p + N_p) F^T]^{-1} F = (S_p + N_p)^{-1}.$$

Then

$$P_i = F S_p (S_p + N_p)^{-1} N_p F^T = F P_p F^T \text{ where } P_p \triangleq S_p (S_p + N_p)^{-1} N_p.$$

P_p is a $p^2 \times p^2$ matrix the diagonal entries of which are repeated in the diagonal of P_i . P_p gives directly the covariance of the gravity gradient at the points of interest.

For the numerical example, we chose a 4 x 4 grid with two different paths and we wish to compare the performances using the criterion mentioned earlier. We have first to define the covariance matrices N and S and to construct the F matrix for the two different paths.

The models used for the random signals n and s are exponentially correlated. That is, the entries of the covariance matrix N_i vary as the exponential of the time difference and the entries of the covariance matrix S_p vary as the exponential of the distance, namely:

$$N_i(i, j) = e^{\frac{-|t_i - t_j|}{\tau}} \text{ and } S_p(i, j) = e^{\frac{-|P_i - P_j|}{\delta}}$$

where τ and δ are correlation time and correlation distance, respectively.

These models do not claim to be accurate but represent only a first try to get numerical performance.

Then we compute $P_p = S_p (S_p + N_p)^{-1} N_p$ to determine the variance of the error associated with the gravity gradient at each point of the grid.

For the two paths, we plot the mean of the standard deviation versus τ ($\tau = 0$ corresponds to a white noise).

Conclusion:

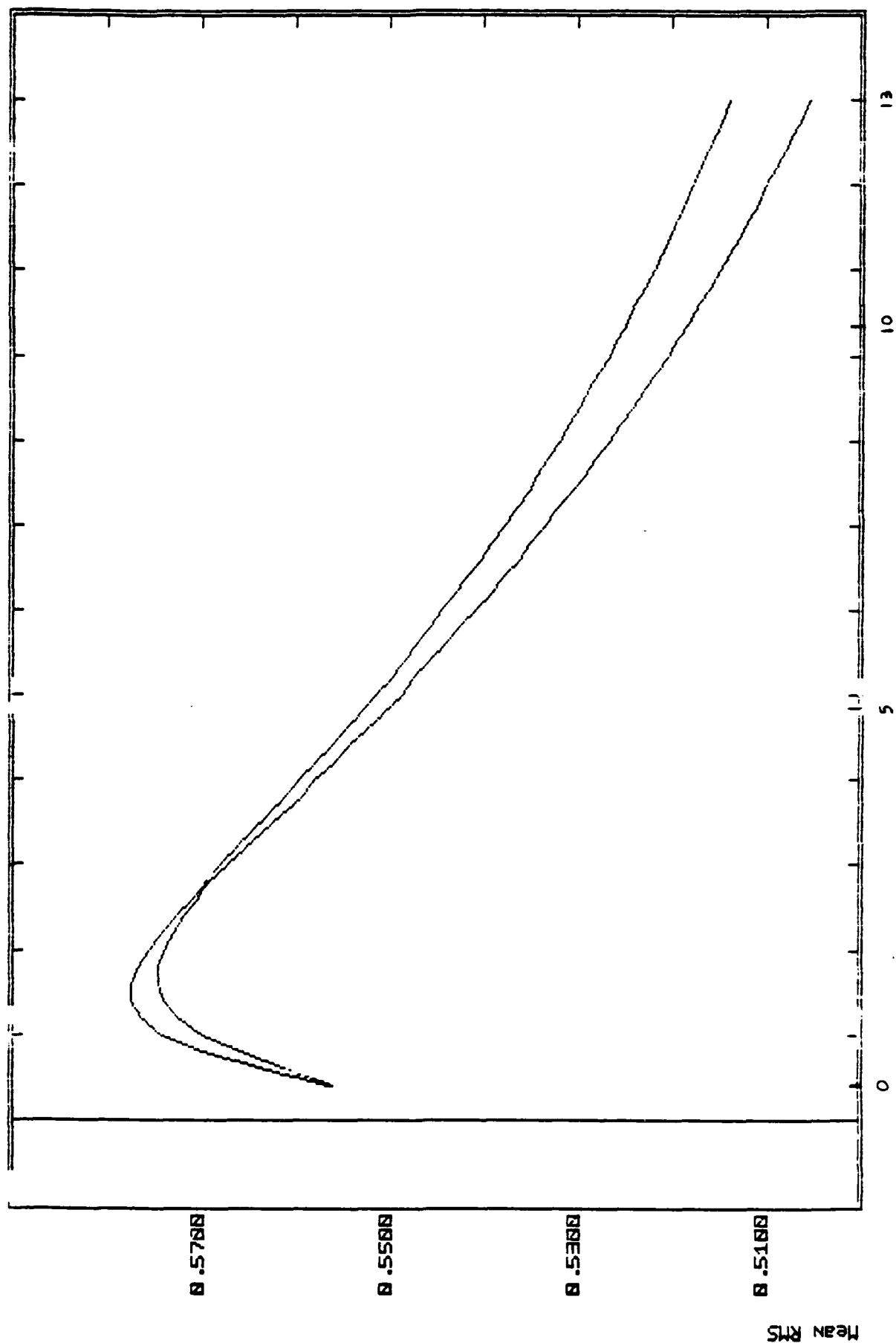
The spectral models of instrument noise and gravity gradient signal we used in our simulations may not be realistic and this marks the limitation of the results we got. However, in the special case of exponential correlated signals, they allow us to answer the question of the best path (among specified ones) according to the criterion we defined. In terms of times of second crossing and times between crossings, the two paths chosen for the simulation can be described as "very" different. Surprisingly enough, the performances for the two paths are close to each other for the range of correlation times we have run.

However, the gap is getting wider in favor of path 1 when the correlation time gets larger but the performance of path 1 is only 1.5 % better for $\tau = 13$ units of time.* In these conditions, the choice of a "better" path appears not to be an issue.

Our final remark concerns the nature of the instrument noise. The way it has been modelled assumed that it was stationary (in particular constant variance at any time); if this is not the case, quite different results may occur; for example, the importance of early crossings increases.

* 1 unit of time is the time required to fly from a point to the next one.

Mean RMS versus Correlation Time of Inst



Correlation time Plot #1 4 Jan-86 20:12

[1] Breakwell, J.V., "Satellite Determination of Short Wavelength Gravity Variations,"
J. of the Astronautical Sciences, No. 4, pp. 329-344, Oct-Dec. 1979.

END

5-87

DTIC